

Experimental Studies in Melting Pyroxenite

Marjorie H. Hirs

Kanani K.M. Lee, Advisor

David Bercovici, Reader

17 December, 2014

A Senior Essay presented to the faculty of the Department of Geology and Geophysics, Yale University, in partial fulfillment of the Bachelor's Degree.

In presenting this essay in partial fulfillment of the Bachelor's Degree from the Department of Geology and Geophysics, Yale University, I agree that the department may make copies or post it on the departmental website so that others may better understand the undergraduate research of the department. I further agree that extensive copying of this thesis is allowable only for scholarly purposes. It is understood, however, that any copying or publication of this thesis for commercial purposes or financial gain is not allowed without my written consent.

Marjorie Hirs, 17 December, 2014

Abstract

The Earth's bulk composition is fundamental to understanding the formation and evolution of Earth. Our experiments aim to investigate the behavior of the Earth's mantle at high pressures and temperatures, so that we may better understand the current state of the Earth's mantle, and its thermochemical evolution over time. Our samples consist of a synthetic garnet pyroxenite mix (MIX 1G, Hirschmann et al., 2003), a bulk composition meant to mimic a plausible source of ocean island basalts (OIB). We use a laser-heated diamond-anvil cell (LHDAC) in order to melt pyroxenite at the lower mantle pressures, in conjunction with 4-color temperature mapping and electron microscopy of quenched samples. Previous LHDAC experiments have looked at the melting curve of peridotite and other plausible lower mantle samples (e.g., [Fiquet et al., 2010]) using x-ray diffraction (XRD) experiments to identify the phases and at what conditions they melt. Our methods differ from previous experiments in that we look to correlate temperature maps with texture images instead of using XRD which can only measure a single peak temperature, thereby possibly overestimating the actual melting temperature. Experiments at increasing pressures (35, 45, and 55 GPa) have yielded liquidus temperatures ranging from 2800 K (35 GPa) to 4800 K (45 GPa).

Introduction

The Earth's lower mantle is the region between the transition zone and the core mantle boundary (CMB). It extends from ~670 km (~25 GPa) down to ~2900 km (~135 GPa) and is characterized by extreme pressure and temperature conditions. Due to the inaccessibility of this region, we must rely on methods such as high-pressure experiments in order to further our understanding of the chemical composition and behavior of the lower mantle. Our LHDAC experiments allow us to recreate pressures and temperatures of the lower mantle, and to place constraints on the behavior of pyroxenite – a possible constituent of the lower mantle as a parent source to OIBs. This allows us to better understand the current state of the Earth's mantle, as well as provide insights to its thermochemical dynamics and evolutions over time.

There is a good geodynamic basis for thinking that pyroxene-rich rocks are recycled into the mantle via subduction. Recycled pyroxene-rich rocks could thus distribute to several mantle reservoirs, such as OIBs, the isotopic signatures of which are the basis for many current models of the evolution of Earth's mantle through time (e.g., [Hofmann 1977], [Hirschmann et al., 2003]).

Geochemical analysis of some OIB suites has recently been used to argue the existence of pyroxenite as an important constituent in OIB source regions. However, direct melting of components found in OIBs leads to magmas compositionally different from the OIBs in which they were found. One possible explanation is that pyroxenites with trace element and isotopic characteristics of subducted materials will yield OIBs. What is more, the compositional variability of mantle pyroxenites could explain the heterogeneity and wide variation in silica content for a given MgO content in alkali OIBs [Hirschmann et al., 2003]. Previous experiments with partial melting of pyroxenites [e.g., Hirschmann et al., 2003], hypothesized that "partial melts of pyroxenites at higher pressures could be more similar to primitive alkalic OIB lavas

than those produced at lower pressures” [Hirschmann et al, 2003]. We hope to expand on this hypothesis by conducting experiments at lower mantle pressure/temperature conditions.

Other LHDAC experiments have looked at the melting curve of peridotite and other samples similar in composition to pyroxenite (e.g., [Fiquet et al., 2010]) (Table 1), at higher pressures. Fiquet et al.’s 2010 experiments with pyrolite, a model rock composition thought to represent the primitive upper mantle [e.g. Ringwood REF], observe its melting behavior at pressures from 36 to 136 GPa.

At greater pressures, our experiments could also provide some insight to ultra-low velocity zones (ULVZs) – thought to be the roots of mantle plumes [Murayama et al., 2007], or remnants of a global magma ocean [McNamara et al., 2010]. ULVZs are small scale (~5-40 km thick and ~km wide) heterogeneities found at the CMB characterized by strong reductions (>10%) in the compressional wave (P-wave) and shear wave (S-wave) velocities relative to the Preliminary Earth Reference Model (PREM). These properties could possibly indicate iron-enriched solid mantle phases [Mao et al., 2006; Wicks et al., 2010], and our preliminary experiments indicate a phase change around 55 GPa which at greater pressures and depth could potentially contribute to the velocity changes seen in the ULVZs.

Our experiments could further our understanding of the origin of silica-undersaturated OIBs, as it is hypothesized that partial melting of pyroxenites are likely parent sources. Additionally, applying the phase diagram of pyroxenite to seismic observations of ULVZs could further promote our understanding of the solid Earth dynamics.

Methods

For our experiments, we used a pyroxenite mixture, glass sample MIX1G [Table 1]; thought to be a potential parent rock for silica-undersaturated OIBs, that is, upon partial melting, MIX1G melts to form an OIB-like composition [Hirschmann et al., 2003].

We used a LHDAC equipped with 300 μm culet diamond anvils. We used precompressed rhenium gaskets in which we drilled a hole in the gasket center (120 μm for the 35 GPa, 165 μm for subsequent pressures), and filled with the glass sample MIX1G [Hirschmann et al., 2003]. To avoid possible contamination from pressure media or calibrants, no other materials were loaded with the sample [e.g., Du & Lee, 2014]. We then closed the cell and brought it up to the desired pressure, using Raman spectroscopy of the diamond edge [Akahama et al., 2006]. At pressures of 35, 45, and 55 GPa, we laser annealed the glass samples by rastering across the samples to convert them to their high-pressure crystalline phases (e.g., Mg-silicate perovskite, also known as brigandite; and stishovite), as well as minimize any deviatoric stresses. To ensure steady heating at the highest temperatures and avoid any thermal runaway common in some LHDAC samples, we used ramped laser heating and monitored the thermal emission [Du et al., 2013, Du & Lee, 2014]. To do this, we heated each sample at a low power (and correspondingly low temperature, ~1500K) for an average of ~2 seconds before ramping up to a higher power and holding it at a single high power for a ~1 second. The temperature was taken just before quenching at the highest power. Thermal emission was monitored continuously throughout the

heating duration. Samples were then pressure checked and photographed, depressurized and unloaded from the DACs.

Temperature and emissivity maps are produced with multi-wavelength imaging radiometry (“4-color” temperature measurement) [Du et al., 2013]. Melting temperature was determined by tracing the perimeter of the melt bleb from the optical image and superimposing the perimeter onto the temperature map [Figs. 1, 2, 3]. By correlating temperature maps with texture images, we were also able to avoid possibly overestimating the actual melt temperature – a drawback of using XRD. We also observe a corresponding jump in emissivity at the corresponding melt temperature, which has been shown to change discontinuously upon melting [Campbell, 2008]. Melting temperature uncertainties are estimated at 7% [Du et al., 2013].

The samples were then prepped for focused ion beam (FIB) to be cross-sectioned. So far, only the sample at 45 GPa has been cross-sectioned. It was then mounted for EDS analysis (Fig. 4). Preliminary analysis shows Fe enrichment of the melt spot, with Ca and Si depletion. Cross-sectioning and EDS analysis is ongoing for the remaining samples.

Results

Preliminary results yield melting temperature of ~4300 K at 35 GPa, and a higher melting temperature of ~4600 K at 45 GPa. However, at 55 GPa, the sample was found to melt at ~3700 K. This suggests a change in the solidus phase at high pressures, consistent with Fiquet et al., 2010, who found that at pressures around 36 GPa, Mg-perovskite melts first while at pressures above 61 GPa, Ca-perovskite and ferropericlasite melt first.

A preliminary EDS analysis of the cross-section of the 45 GPa melt spot indicated Fe going into the melt, also consistent with previous results [e.g., Fiquet et al., 2010, Du & Lee, 2014] and suggestive of an Mg-perovskite solidus phase. FIB cross-sectioning treatment and EDS analysis are still ongoing for the other two samples. This will show whether or not the solidus phase does change as is expected given the drop in the temperature of the melt feature.

Conclusions and Future Work

Currently, until our samples can be observed in cross-section and analyzed by EPMA, the solidus phase identity has yet to be determined and will likely change with pressure. Basing our expectations off of Fiquet et al., 2010, we would then expect to see a change from solidus of Mg- and Ca-perovskite (CaSiO₃) to a solidus of ferropericlasite (Mg, Fe)O happening around these pressures.

This phase change has implications for both the understanding of the origin of silica depleted OIBs and for being a possible explanation or contributing factor to the velocity reductions seen in ULVZs. The change in solidus phase could explain the compositional discrepancies previously found when testing pyroxenite as a plausible parent source for OIBs [Hirschmann et al., 2003]. It could also explain velocity reductions in ULVZ as a potential explanation for wave velocity diminishment is enrichment of Fe in the solid mantle phases.

The goal of this work is to further our understanding of lower mantle processes by establishing a melting curve of pyroxenite, which could have implications for both the formation and the origins of OIBs as well as provide insight and explanation to the velocity reductions in ULVZs. In order to do this we would need to obtain melt samples at higher pressures in increments of 10 GPa from 65 GPa up to 135 GPa (CMB pressure). Through analysis of further samples, we would hope to construct a phase diagram of relevant phases over the PT range of the lower mantle. This work is in progress and from preliminary results seems promising.

Acknowledgments

This work was funded in part by the Von Damm undergraduate Fellowship and NSF CAREER grant to K. K. M. Lee (EAR-0955824). FIB use was supported by YINQE and NSF MRSEC DMR 1119826, and carried out in part at the Center for Functional Nanomaterials, Brookhaven National Laboratory, which is supported by the U.S. Department of Energy, Office of Basic Energy Sciences, under Contract No. DE-AC02-98CH10886. We acknowledge the technical assistance of Zhixue Du, Zhenting Jiang, Michael Rooks, Fernando Camino and George Amulele.

References Cited

- Akahama, Y. and H. Kawamura, *J. Appl. Phys.*, 100, (2006).
- Campbell, A. J., *Rev. Sci. Inst.*, 79, 015108 (2013).
- Du, Z., G. Amulele, L. R. Benedetti and K. K. M. Lee, *Rev. Sci. Inst.*, 84, 075111 (2013).
- Hirschmann, M. M., T. Kogiso, M. B. Baker and E. M. Stopler, *Geology*, 31, 6, 481–484 (2003).
- Fiquet, G., A. L. Auzende, J. Siebert, A. Corgne, H. Bureau, H. Ozawa and G. Garbarino, *Science* 329, 1516 (2010).
- Javoy, M., *Geophys. Res. Letts.*, 22, 16, 2219-2222 (1995).
- Mao, W. L. *et al.* Iron-rich post-perovskite and the origin of ultralow-velocity zones. *Science* **312**, 564–565 (2006).
- McDonough, W. F. and S.-s. Sun, *Chemical Geology*, 120, 223-253 (1995).
- McNamara, A.K., E.J. Garnero, and S. Rost, Tracking deep mantle reservoirs with ultra low velocity zones, *Earth and Planetary Science Letters*, 299, 1-9, 2010.
- Sh. Maruyama, D. A. Yuen, and B. F. Windley, “Dynamics of Plumes and Superplumes Trough Time,” in *Superplumes: Beyond Plate Tectonics*, Ed. by D. A. Yuen, Sh. Maruyama, Sh. I. Karato, and B. F. Windley (Springer, Dordrecht, 2007), pp. 441–502.
- S.M. Dorfman and T.S. Duffy, Effect of Fe-enrichment on seismic properties of perovskite and post-perovskite in the deep lower mantle, *Geophys. J. Int.* 2014 197: 910-919.

Supplement

Figures and Tables

Figures 1, 2, 3. Melting of sample MIX 1G at 35, 45, and 55 GPa. For each pressure, clockwise from top left: (A) Optical image of melted sample. (B) 2-D temperature map. (C) Temperature-emissivity transects across the center. (D) 2-D emissivity map. Melting temperature was determined by tracing the perimeter of the melt bleb from the optical image and superimposing the perimeter onto the temperature map. We also observe a corresponding jump in emissivity at the corresponding melt temperature (shown with shaded rectangle), which has been shown to change discontinuously upon melting [Campbell, 2008]. Melting temperature uncertainties are estimated at 7% [Du et al., 2013].

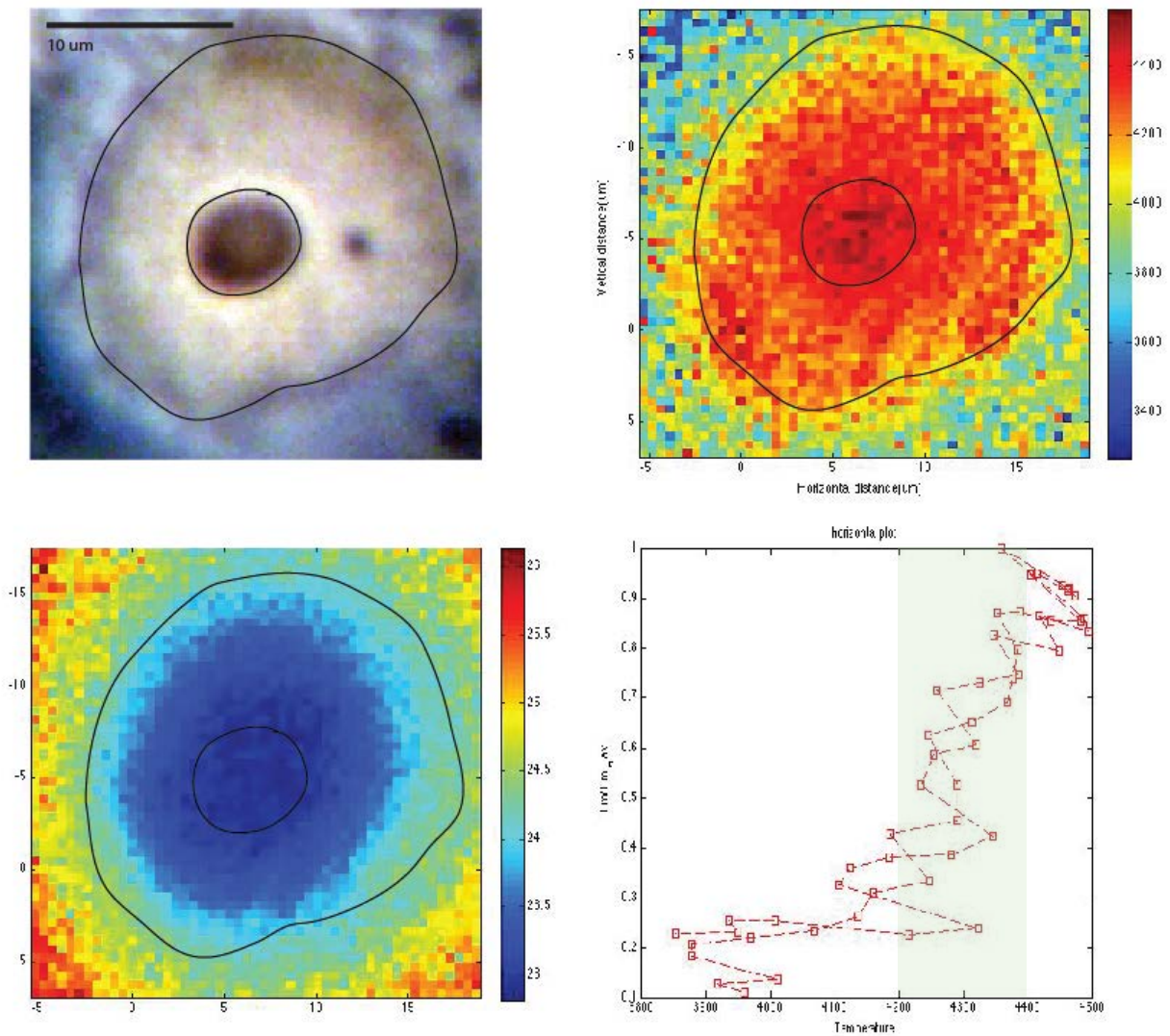


Figure 1 - 35 GPa

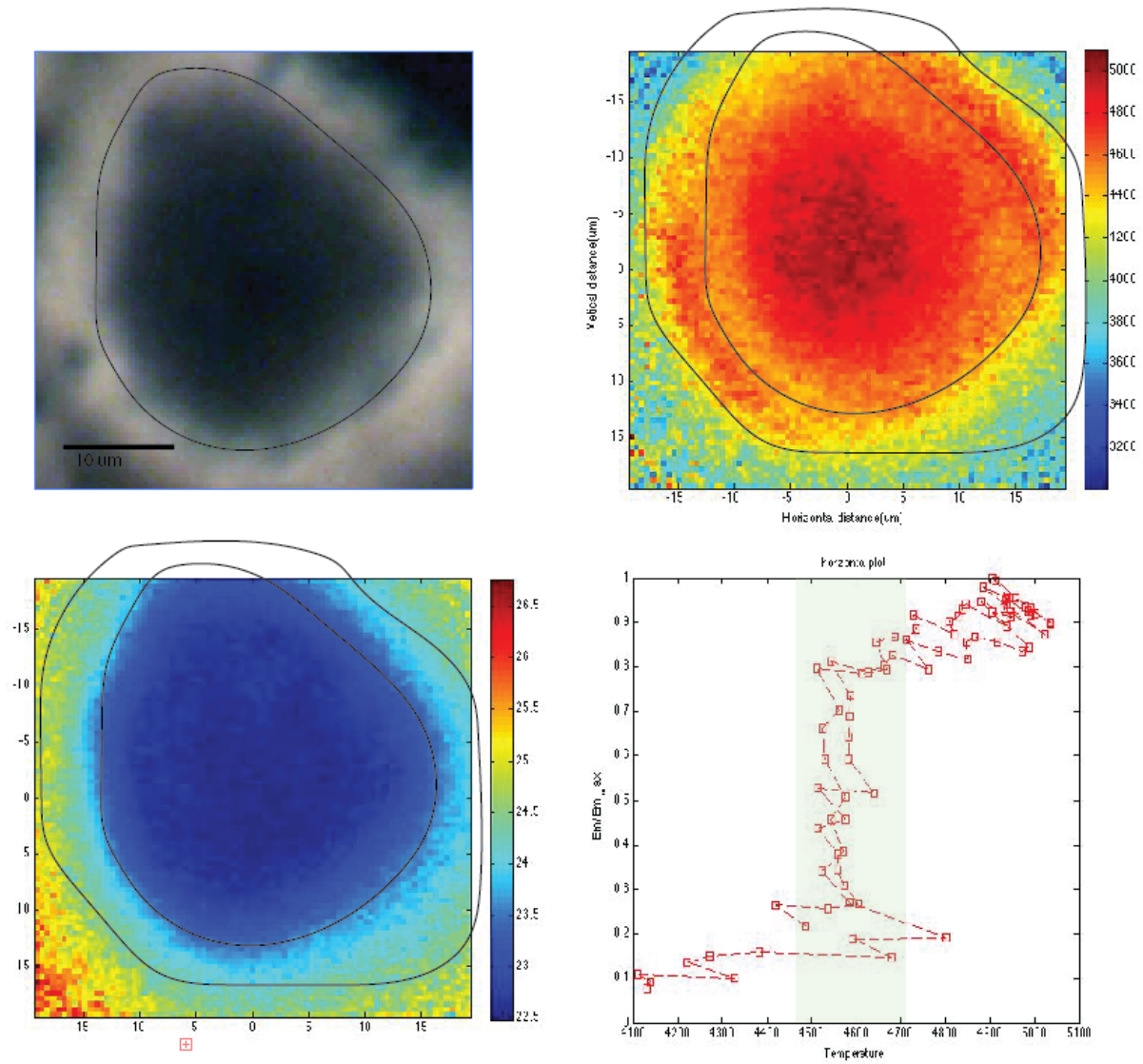


Figure 2 - 45 GPa

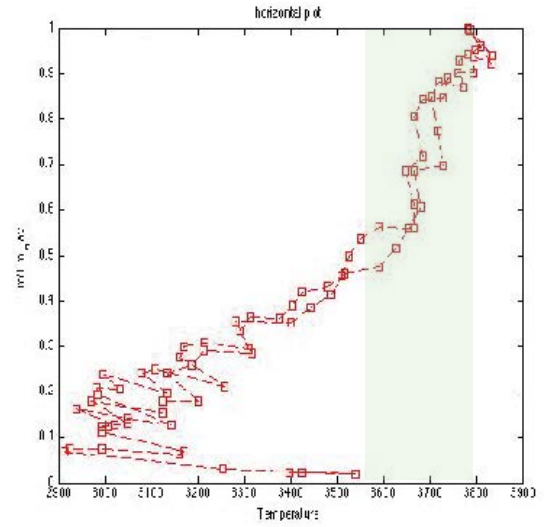
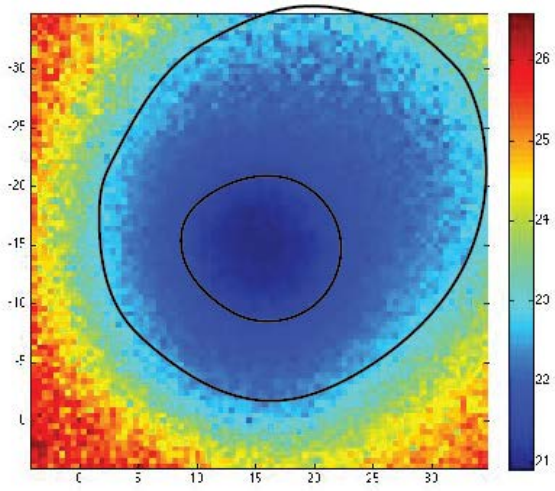
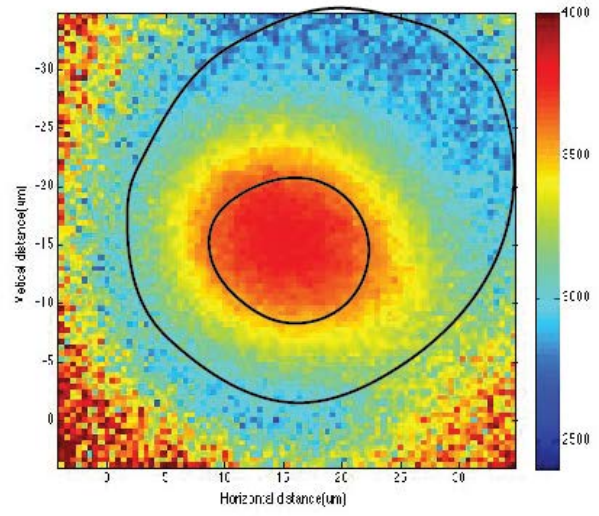
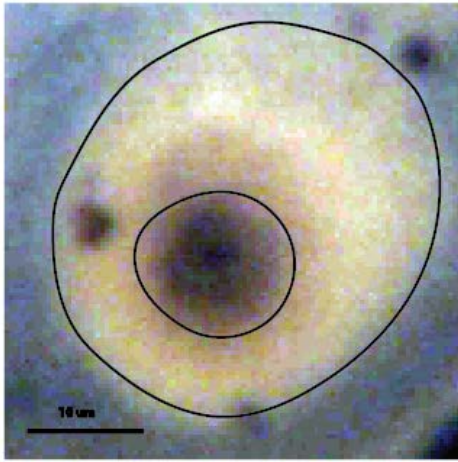


Figure 3 - 55 GPa

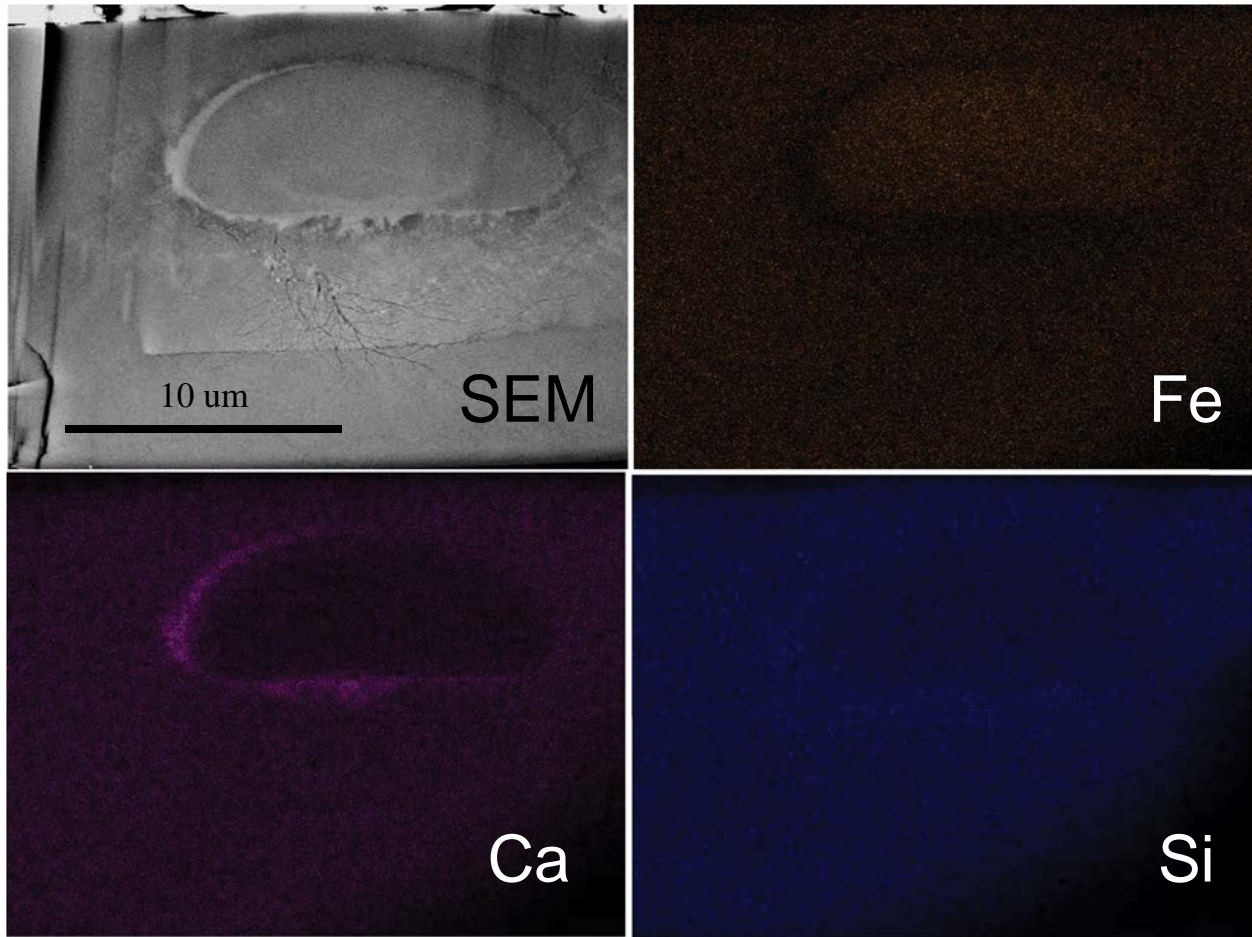


Figure 4 - (Top Left) SEM image of melt spot cross section at 45 GPa. (Clockwise from top right) Fe, Si, and Ca concentration maps of heated area by EDS. Melt perimeter shows division between Fe and Ca/Si – rich areas.

Table 1. Data is shown in mol%, normalized to 100%. ^All Fe is listed as FeO. For comparison, a pyrolite and enstatite LM chondrite compositions are shown.

MgO	SiO ₂	Al ₂ O ₃	CaO	FeO [^]	(Mg+Fe)/Si	Reference
24.7	45.4	8.9	12.2	6.5	0.687	MIX 1G, [Hirschmann et al., 2003]
36.6	47.2	2.2	1.6	12.4	1.038	Enstatite Chondrite LM, [Javoy, 1995]
49.3	39.4	2.3	3.1	5.9	1.401	Pyrolite, [McDonough & Sun, 1995]

Methods

35 GPa: All heating was of the flat side of the DAC as the hemisphere side presented a small mark and we wanted to avoid any further damage that might be caused by heating through that side. We annealed the sample starting at 10% up to 20% power with no ND filter in place. Once sufficiently preheated, we checked cell pressure and set up the cell again to be heated. Four spots were made: spot A with ND filter 1 in place, peak power of 36 and exposure time of .01s, spot B with ND filter 1 in place, peak power of 37, and exposure time of 0.01s, spot C with ND filter 1 in place, peak power of 39, and exposure time of 0.01 s, and spot D with ND filter 1 in place, peak power of 40 and exposure time of 0.01s. Spot D exhibited unsteady heating.

45 GPa: New diamonds were loaded into the DAC. We annealed up to 22% on the flat side of the DAC before we began annealing from both sides at lower power. Heating was one-sided. We made four spots: spot A preheating at 20, with peak power at 40 and exposure time of 0.01s (Spot A was no good though because we left the laser on while taking a white light image), spot B with ND filter 1, preheating at 30, with peak power at 50, and exposure time of 0.01s - we then reheated up to 60 in the same spot, spot C with ND filter 1, preheating at 30, with peak power at 70, and exposure time of 0.01s, spot D with ND filter 1, preheating at 30, with peak power at 60, and exposure time of 0.01s, and spot E with ND filter 1, preheating at 30 with peak power at 55, and exposure time of 0.01s.

55 GPa: We annealed from both sides of the DAC at 16%. We made 5 spots all with ND filter 1 in place: spot A preheating at 16% for 2s ramping up to 30% at 3s with total duration of 3.5s and exposure time of 0.1.s, spot B preheating at 20% up to 40% with exposure time of 0.1s, spot C preheating at 20% up to 42% with exposure time of 0.05s, spot D preheating at 20% up to 42% with exposure time of 0.1s, and spot E preheating at 20% up to 44% with exposure time of 0.05s.